

## Theoretical Study of Aqueous Solvation of $K^+$ Comparing *ab Initio*, Polarizable, and Fixed-Charge Models

Troy W. Whitfield,<sup>†</sup> Sameer Varma,<sup>§</sup> Edward Harder,<sup>||</sup> Guillaume Lamoureux,<sup>‡</sup>  
Susan B. Rempe,<sup>\*,§</sup> and Benoit Roux<sup>\*,||</sup>

*Biosciences Division, Argonne National Laboratory, 9700 South Cass Avenue,  
Argonne, Illinois 60439, Center for Molecular Modeling and Department of Chemistry,  
University of Pennsylvania, Philadelphia, Pennsylvania 19104-6323,  
Computational Bioscience Department, Sandia National Laboratories,  
Albuquerque, New Mexico 87185, and Department of Biochemistry,  
University of Chicago, Chicago, Illinois 60615*

Received July 11, 2007

**Abstract:** The hydration of  $K^+$  is studied using a hierarchy of theoretical approaches, including *ab initio* Born–Oppenheimer molecular dynamics and Car–Parrinello molecular dynamics, a polarizable force field model based on classical Drude oscillators, and a nonpolarizable fixed-charge potential based on the TIP3P water model. While models based more directly on quantum mechanics offer the possibility to account for complex electronic effects, polarizable and fixed-charges force fields allow for simulations of large systems and the calculation of thermodynamic observables with relatively modest computational expense. A particular emphasis is placed on investigating the sensitivity of the polarizable model to reproduce key aspects of aqueous  $K^+$ , such as the coordination structure, the bulk hydration free energy, and the self-diffusion of  $K^+$ . It is generally found that, while the simple functional form of the polarizable Drude model imposes some restrictions on the range of properties that can simultaneously be fitted, the resulting hydration structure for aqueous  $K^+$  agrees well with experiment and with more sophisticated computational models. All the computational models yield a similar hydration structure, with a first peak in the radial distribution function near 2.7 Å, though the distribution functions obtained from the two *ab initio* simulations are less sharply peaked. A counterintuitive result, seen in Car–Parrinello molecular dynamics and in simulations with the Drude polarizable force field, is that the average induced molecular dipole of the water molecules within the first hydration shell around  $K^+$  is slightly smaller than the corresponding value in the bulk. In final analysis, the perspective of  $K^+$  hydration emerging from the various computational models is broadly consistent with experimental data, though at a finer level there remain a number of issues that should be resolved to further our ability in modeling ion hydration accurately.

### I. Introduction

Small ions such as  $K^+$  and  $Na^+$  play a ubiquitous role in biology. For this reason, understanding how they are solvated

by water molecules remains an issue of great relevance. A powerful approach to investigate ion solvation is to rely on computer simulations of atomic models based on potential functions.<sup>1–5</sup> For meaningful simulation studies it is important to use models that represent the microscopic interactions as accurately as possible. In the past few decades, a number of fixed-charge nonpolarizable force fields have been parametrized to model ion solvation<sup>6–9</sup> and are now used on a regular basis to investigate diverse problems. Induced

\* Corresponding author e-mail: roux@uchicago.edu (B.R.),  
slrempe@sandia.gov (S.B.R.).

<sup>†</sup> Argonne National Laboratory.

<sup>‡</sup> University of Pennsylvania.

<sup>§</sup> Sandia National Laboratories.

<sup>||</sup> University of Chicago.

electronic polarization, which is generally neglected in standard molecular dynamics simulations of biomolecular systems, remains of particular concern in the case of ionic systems where nonadditive many-body effects could be important. In principle, accurate computational models can be developed, validated, and refined by comparing with experimental data (gas and bulk phase) as well as high level *ab initio* computations. In practice, however, this presents a difficult challenge for a number of reasons.

The individual microscopic interactions that are involved in ion hydration are most directly probed by single-ion thermochemical gas-phase experimental data on small water clusters.<sup>10–12</sup> Nonetheless, how this information must be extrapolated to the bulk phase is uncertain, because the properties of small clusters can be both similar and different from their bulk counterparts. Interpretation of experimental data about ions in the bulk phase is also not without any difficulties. Analysis of the neutron scattering data used to measure the coordination structure of  $\text{Na}^+$  and  $\text{K}^+$  in liquid water must rely on simulation models to determine the partial radial distribution functions.<sup>13</sup> These problems are reflected in the lack of consensus concerning the structural properties of hydrated ions, especially their hydration numbers.<sup>14</sup> An additional piece of information in developing meaningful ion solvation models is the experimentally measured hydration free energies. Experimental determination of the hydration free energies of charged species is a challenging problem that has been revisited numerous times over the years.<sup>4,5,12,15–20</sup> Single ion solvation properties in the infinite dilution limit must be extracted from electrochemical data using extra-thermodynamic assumptions, which are uncertain.<sup>5</sup> These difficulties are further compounded by the fact that, in a real physical system, the total reversible work to take an ion from the gas phase and transfer it into a bulk liquid phase includes a contribution from the electrostatic potential associated with the vacuum/liquid interface. The currently available experimental data are, by themselves, insufficient to establish a definitive picture of the solvation of simple ions such as  $\text{K}^+$  and  $\text{Na}^+$  in water.

Computations can be used to extend the information extracted from experiments. Because they can account for a wide range of complex electronic effects, simulations based on quantum mechanical *ab initio* methods offer an important source of information to deepen and extend our knowledge of ion solvation. However, bulk phase *ab initio* simulations are computationally intensive and can be burdened by finite size effects, short sampling time, and any approximations inherent to the treatment of electron correlation. In the particular case of density functional theory (DFT), approximations in available exchange-correlation functionals and the neglect of van der Waals dispersive attraction must also be kept in mind.<sup>21–23</sup> Alternatively, simulations based on physically realistic classical potential functions offer a path for estimating statistically converged thermodynamic averages, in terms of size and configurational sampling, although the validity of the simplifying assumptions upon which these potential functions are constructed must be assessed. In spite of these difficulties, it is our hope that a well-defined (if not definitive) perspective on the aqueous

solvation of small ions can emerge by critically examining and contrasting data from simulations and experiments.

In the present effort, aqueous solvation of  $\text{K}^+$  is investigated using a hierarchy of computational approaches. This includes two quantum mechanical *ab initio* simulation methods, Born–Oppenheimer molecular dynamics (BOMD) and Car–Parrinello molecular dynamics (CPMD), as well as two classical force field methods, TIP3P, a widely used nonpolarizable effective fixed charge model,<sup>8,24</sup> and SWM4-NDP, a polarizable model based on classical Drude oscillators.<sup>25</sup> The polarizable model of ion solvation presented here is based upon the classical Drude oscillator.<sup>26–31</sup> In this model, electronic induction is represented by the displacement of a charge-carrying auxiliary particle harmonically bound to a polarizable atom under the influence of the local electric field. The familiar self-consistent field (SCF) regime of induced polarization is reproduced in molecular dynamics simulations if the classical Drude oscillators are kept near their local energy minima for a given configuration of the atoms in the system.<sup>31</sup>

In the following, the ability of the models to reproduce the single-ion thermochemical gas-phase data in small clusters is examined. In addition, a particular emphasis is placed on examining the sensitivity in the Drude model of key aspects of aqueous solvation of  $\text{K}^+$ , such as the coordination structure, the hydration free energy, and the coefficient of self-diffusion. It is found that, while the simple functional form of potential functions imposes some restrictions on the range of properties that can simultaneously be fitted, the resulting hydration structure for aqueous  $\text{K}^+$  is in broad accord with experiment and with *ab initio* simulations. In conclusion, MD studies based on properly parametrized models can yield meaningful results, although there remain a number of small discrepancies that shall be critically examined.

## II. Methods

The hydration of  $\text{K}^+$  was studied using four distinct computational models, the details of which are outlined below. The four computational models are as follows: (i) a fixed charge model based upon the TIP3P<sup>24</sup> water model, (ii) a Drude polarizable model based upon the SWM4-NDP water model,<sup>25</sup> (iii) a density functional theory (DFT) model based upon the gradient-corrected PW91 approximate density functional,<sup>32,33</sup> and (iv) a second DFT model using the gradient-corrected BLYP approximate density functional.<sup>34,35</sup> In all periodic simulations with a net charge, a uniform canceling background charge is assumed.

**A. Fixed Charge Model.** The fixed charge model of aqueous  $\text{K}^+$  is based on the Lennard-Jones parameters that were previously optimized<sup>8</sup> to give reasonable monohydrate energy and hydration free energies for  $\text{K}^+$  when used in conjunction with the TIP3P water model;<sup>24</sup> the parameters for  $\text{K}^+$  are  $E_{\text{min}} = 0.0870$  kcal/mol, and  $\sigma = 2.142645$  Å assuming a Lorentz–Berthelot combination rule with the TIP3P parameters. A system consisting of a box of 500 TIP3P water molecules and a single  $\text{K}^+$  ion was simulated with periodic boundary conditions. Long-range electrostatic interactions were computed using Ewald summation.<sup>36</sup> The

canonical ensemble was simulated using Nosé-Hoover thermostats<sup>37</sup> and a 1 fs time-step. The internal geometry of the TIP3P water molecule was fixed using the SHAKE<sup>38</sup> algorithm. After an initial equilibration of 100 ps, equilibrium properties were averaged over a 1 ns molecular dynamics simulation.

**B. Drude Polarizable Model.** The model for  $K^+$  is consistent with the recently developed SWM4-NDP polarizable water model with a negatively charged Drude oscillator bound to its oxygen site.<sup>25</sup> The SWM4-NDP potential reproduces most properties of bulk water under ambient conditions (density, vaporization enthalpy, radial distribution function, dielectric constant, self-diffusion constant, shear viscosity, and free energy of hydration). In particular, the SWM4-NDP model yields a correct static dielectric constant, which makes it appropriate to study systems dominated by water-mediated electrostatic interactions. Accordingly, polarization of the cation is represented with a negatively charged particle bound to its nucleus. All atomic dispersion and electronic overlap effects are represented in a pairwise additive way using the Lennard-Jones potential.

The interaction energy of a single ion of charge  $q_{\text{ion}}$  with  $N$  water molecules is

$$U_{\text{iw}}(\mathbf{r}_{\text{is}}, \mathbf{r}, \mathbf{r}_{\text{D}}) = \frac{1}{2} k_{\text{D}} |\mathbf{r} - \mathbf{r}_{\text{D}}|^2 + \sum_{i=1}^N \sum_{s=1}^4 \left[ \frac{(q_{\text{ion}} - q_{\text{D}}) q_s}{|\mathbf{r} - \mathbf{r}_{\text{is}}|} + \frac{q_{\text{D}} q_s}{|\mathbf{r}_{\text{D}} - \mathbf{r}_{\text{is}}|} \right] + \sum_{i=1}^N 4\epsilon_{\text{ion-O}} \left[ \left( \frac{\sigma_{\text{ion-O}}}{|\mathbf{r} - \mathbf{r}_{\text{io}}|} \right)^{12} - \left( \frac{\sigma_{\text{ion-O}}}{|\mathbf{r} - \mathbf{r}_{\text{io}}|} \right)^6 \right] \quad (1)$$

where the vectors  $\mathbf{r}$  and  $\mathbf{r}_{\text{D}}$  are the positions of the ionic core and the ionic Drude particle, respectively. The ionic core has a charge  $(q_{\text{ion}} - q_{\text{D}})$  and the Drude particle has a charge  $q_{\text{D}}$ . The spring constant  $k_{\text{D}}$  is set to 1000 kcal/mol/Å<sup>2</sup> for all Drude oscillators in the system. This value dictates the magnitude of the charge the Drude particle should carry to produce an ionic polarizability  $\alpha$ , i.e.,  $q_{\text{D}} = -\sqrt{\alpha k_{\text{D}}}$ .<sup>25</sup> In eq 1, the vector  $\mathbf{r}_{\text{is}}$  is the position of the interaction site  $s$  of water molecule  $i$ . The SWM4-NDP water model comprises five sites: the oxygen atom “O” (charge =  $-q_{\text{D}}$ ), the hydrogen atoms “H<sub>1</sub>” and “H<sub>2</sub>” (charged), a massless site “M” (charged), and a Drude particle “D” attached to the oxygen atom (negatively charged). The Lennard-Jones parameters for the ion–water oxygen interaction are determined via the Lorentz–Berthelot combination rule,<sup>39</sup>  $\epsilon_{\text{ion-O}} = \sqrt{\epsilon_{\text{ion}} \epsilon_{\text{O}}}$  and  $\sigma_{\text{ion-O}} = (\sigma_{\text{ion}} + \sigma_{\text{O}})/2$ . The parameters for  $K^+$  were chosen to give agreement with experimental monohydrate properties<sup>10</sup> and a hydration free energy for the cation that was consistent with published values.<sup>5,40,41</sup>

The simulation protocol for studying the bulk hydration structure of the polarizable Drude model is identical to that of the fixed charge model, except that a dual thermostat scheme was used to keep the Drude particles at a low temperature (1 Kelvin) and therefore close to the (self-consistent field) ground state.<sup>31</sup>

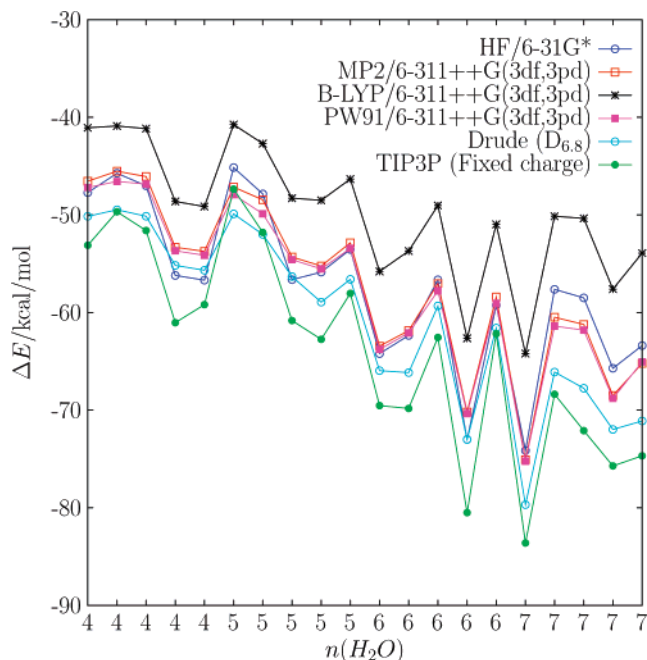


**Figure 1.** Interaction energies for a series of  $K^+$  ( $H_2O$ )<sub>*n*</sub> clusters at various levels of ab initio theory and for a fixed charge and Drude polarizable model. Each cluster was extracted from MD simulation of aqueous  $K^+$ . The x-axis indexes the number of water molecules,  $n$ , coordinating the cation.

The adjustable parameters for monatomic ions within the classical Drude scheme to build a polarizable biomolecular force field are the Lennard-Jones parameters of the ion,  $\sigma_{\text{ion}}$  and  $\epsilon_{\text{ion}}$ . Rather than try to determine these parameters by scanning in the space of  $\{\sigma_{\text{ion}}, \epsilon_{\text{ion}}\}$ , it has proved more convenient to explore the space of monohydrate interaction energies and minimum-energy ion–oxygen distances  $\{U_{\text{min}}, d_{\text{min}}\}$ .<sup>5</sup> Furthermore, quadratic response functions are fitted to the data from explicit computations, defined by coordinates in  $\{U_{\text{min}}, d_{\text{min}}\}$ , to interpolate predicted properties between simulated models.<sup>5,25</sup> A set of polarizable models for  $K^+$  were thus constructed by determining the Lennard-Jones parameters spanning a regular grid in the  $\{U_{\text{min}}, d_{\text{min}}\}$  coordinates. For each model on the grid, MD simulations were then carried out to compute the aqueous bulk hydration number,  $n(r_c)$ , and the bulk hydration free energy,  $\Delta G_{\text{hydr}}$ . These properties were then fitted to a polynomial response function with a quadratic dependence on  $\{U_{\text{min}}, d_{\text{min}}\}$ . The results of these computations are summarized in Figures 2 and 3. To monitor consistency between  $K^+$  and  $Na^+$  models, the hydration free energy of  $Na^+$  is also reported in Figure 4 for a set of  $Na^+$  polarizable Drude models.

The hydration free energy of the ions was decomposed into three contributions<sup>42</sup>

$$\Delta G_{\text{hydr}} = \Delta G_{\text{hydr}}^{\text{rep}} + \Delta G_{\text{hydr}}^{\text{disp}} + \Delta G_{\text{hydr}}^{\text{elec}} \quad (2)$$

where  $\Delta G_{\text{hydr}}^{\text{rep}}$  and  $\Delta G_{\text{hydr}}^{\text{disp}}$  are the repulsive and attractive (dispersive) components, respectively, of the Lennard-Jones interaction in eq 1. The electrostatic component of the hydration free energy is  $\Delta G_{\text{hydr}}^{\text{elec}}$ . Each component of the total hydration free energy was computed from independent



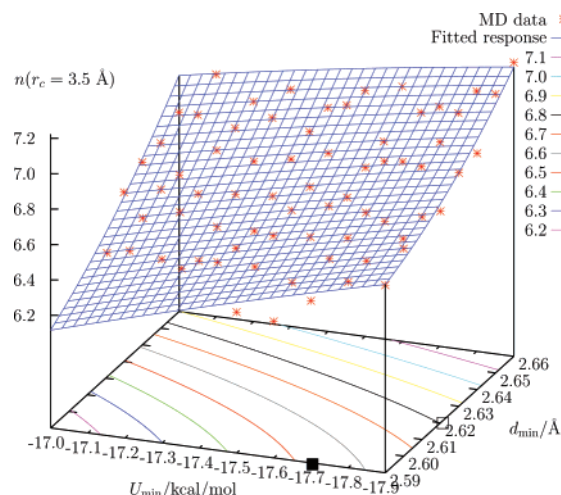


**Figure 2.** Coordination number,  $n(r_c = 3.5 \text{ \AA})$ , for a family of putative  $\text{K}^+$  ions as a function of monohydrate properties for the polarizable model. The open square ( $\square$ ) indicates the location of the  $\text{D}_{6.8}$  model, while the filled square ( $\blacksquare$ ) indicates that of the  $\text{D}_{6.5}$  model.

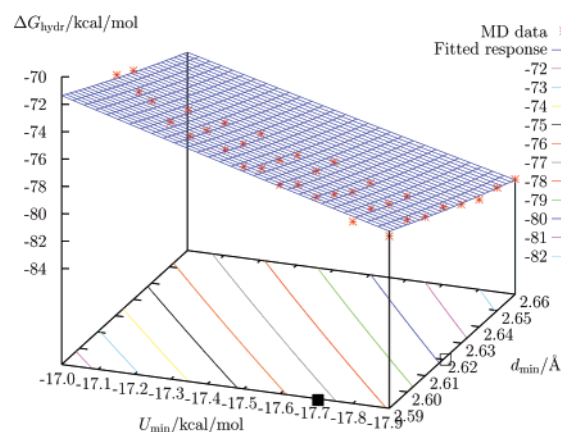


**Figure 3.** Computed hydration free energy for a family of putative  $\text{K}^+$  ions as a function of monohydrate properties for the polarizable model. The open square ( $\square$ ) indicates the location of the  $\text{D}_{6.8}$  model, while the filled square ( $\blacksquare$ ) indicates that of the  $\text{D}_{6.5}$  model.

simulations in which an ion was placed at the center of a droplet of 200 explicit SWM4-NDP water molecules, contained by the reactive spherical solvent boundary potential (SSBP).<sup>8</sup> The repulsive contribution,  $\Delta G_{\text{hydr}}^{\text{rep}}$ , was computed using a soft-core scheme as described elsewhere<sup>42</sup> and was unbiased using the weighted histogram analysis method (WHAM),<sup>43</sup> while  $\Delta G_{\text{hydr}}^{\text{disp}}$  and  $\Delta G_{\text{hydr}}^{\text{elec}}$  were computed using thermodynamic integration (TI). In discussions of the hydration free energies of ionic species, one may consider the *real* physical value, which includes the contribution of the phase potential arising from crossing the physical air/water interface, and the *intrinsic* bulk-phase value, which is independent of any interfacial potential.<sup>5,18</sup> Because the interfacial potential in SSBP is nearly identical to the one from a simulation of a vacuum-liquid interface,<sup>5</sup> the charging free energy computed with SSBP effectively includes the interfacial potential contribution that an ion gains by crossing the physical interface from the gas phase to the bulk water.

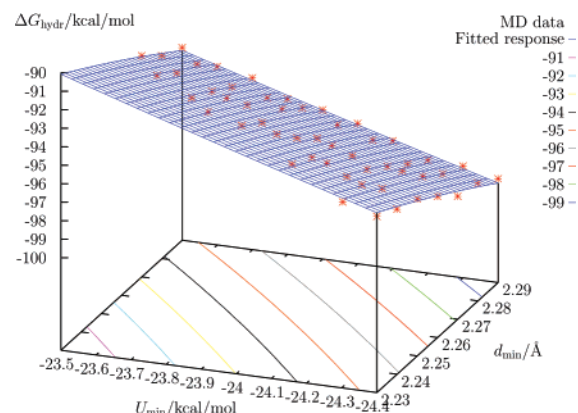


**Figure 4.** Computed hydration free energy of  $\text{Na}^+$  as a function of monohydrate properties for the polarizable model.

It follows that the results from SSBP computations can readily be interpreted as *real* hydration free energies. Unless specified otherwise, *real* hydration free energies are discussed in the rest of the paper.

For convenience, the upper bound on the radial integral used throughout to define the hydration number was set to  $r_c = 3.5 \text{ \AA}$ . While this choice for  $r_c$  may not always coincide with the conventional definition that  $r_c$  is the position of the first minimum in the radial distribution function for the  $\text{O}-\text{K}^+$  contact in all of the models of aqueous  $\text{K}^+$  studied here, it is necessary when comparing so many different models. As it turns out,  $r_c = 3.5 \text{ \AA}$  is a good approximation for the position of the first minimum in  $g_{\text{OK}^+}(r)$  for all of the Drude models, the fixed charge model and the PW91/pw representation of the system. Since the only radial distribution function examined here is for the  $\text{O}-\text{K}^+$  contact, the definitions  $g_{\text{OK}^+}(r) \equiv g(r)$  and  $n_{\text{OK}^+}(r) \equiv n(r)$  are employed in the remainder of this paper.

**C. Ab Initio Models.** The fixed charge and Drude polarizable models of aqueous  $\text{K}^+$  are compared with two different ab initio density functional theory (DFT) models of the same system, each using a different gradient-corrected approximate density functional: BLYP<sup>34,35</sup> and PW91.<sup>32,33</sup> Although both ab initio simulations were performed at the  $\Gamma$ -point, there are many methodological differences between the two computations. Simulations with the PW91 exchange-correlation functional were performed within a Born–Oppenheimer molecular dynamics (BOMD) scheme using the VASP software package,<sup>44,45</sup> while simulations using the BLYP functional were performed within the Car–Parrinello molecular dynamics scheme<sup>46</sup> using the PINY\_MD software package.<sup>47,48</sup> Some results from this BOMD simulation have previously been published elsewhere.<sup>14,49</sup> The simulation details are given below.

In the BOMD simulation of aqueous  $\text{K}^+$ , core-valence interactions are described using the projector augmented-wave (PAW) method.<sup>50,51</sup> Convergence was accepted for the electronic structure calculation when the energy difference between successive self-consistent iterations is less than  $10^{-6}$  eV and the valence orbitals are expanded in plane waves with a kinetic energy cutoff of 36.75 Ry (500 eV). This model of the aqueous  $\text{K}^+$  system is henceforth referred to as PW91/pw.

The system consisted of 64 water molecules and one  $K^+$  ion in a cubic box of length 12.4171 Å with periodic boundary conditions. The fixed volume was chosen such that the water density matches the experimental density of liquid water at standard conditions. Initial conditions come from a well-equilibrated classical MD run of pure liquid water at standard conditions using SPC/E<sup>52</sup> water for 20 ps, followed by a 10 ps BOMD simulation of pure water. In the BOMD simulation of pure water, a Nosé-Hoover thermostat was applied to constrain the temperature to 375 K, after which a  $K^+$  ion was inserted into the box of pure water and all hydrogens were deuterated. The 3p semicore electrons were explicitly included in the valence orbitals for  $K^+$  ion. During the equilibration phase, constant temperature was maintained at  $T = 330$  K with velocity scaling and the equations of motion were integrated using a 1 fs time-step for 14.5 ps. The equilibrated system was then simulated in the micro-canonical ensemble with a 0.5 fs time-step for 40 ps of production. During the course of the BOMD simulation, the temperature was  $313 \pm 21$  Kelvin.

The CPMD simulations of aqueous  $K^+$  used the gradient-corrected BLYP approximate density functional<sup>34,35</sup> and a plane-wave basis set. Calculations were performed with a 70 Ry energy cutoff and norm-conserving pseudopotentials.<sup>53</sup> Following the prescription of the initial fully ab initio simulations carried out on this system,<sup>54</sup> the semicore 3 *s* and 3 *p* states of potassium have been included with the valence electrons. A baseline fictitious electronic mass of 475 au was used with mass preconditioning.<sup>55</sup> The canonical ensemble was sampled using Nosé-Hoover chain thermostats<sup>37,56–59</sup> and a 0.125 fs time-step. In order to ensure adiabaticity, the hydrogen masses were substituted with oxygen masses. The temperature over the course of the CPMD simulation was  $296 \pm 15$  Kelvin. This model of the aqueous  $K^+$  system is henceforth referred to as BLYP/pw.

The BLYP/pw system consisted of the same equilibrated BOMD simulation box as above, containing 64 water molecules with a single potassium cation and with periodic boundary conditions. The system was further equilibrated for 5 ps of CP molecular dynamics. Results were collected during a subsequent 50 ps CPMD simulation. An error analysis and finite system size study for this small system and the relatively short simulation times of the ab initio systems presented in the Appendix indicate that the simulations are statistically accurate and representative of the properties of a system with a large number of water molecules (no significant finite size effect on the ion–water radial distribution function).

### III. Results and Discussion

**A. Monohydrate and Cluster Energies.** The interaction energy of the  $K^+$  monohydrate was computed with various methods. The geometry of the monohydrate was optimized for the fixed charge and polarizable Drude models using the CHARMM<sup>60</sup> software package and also quantum mechanically at the Hartree–Fock level with the 6-31G\* basis set. In each case the  $K^+$  ion was coplanar with the plane of the water molecule, coordinated with the oxygen atom (that is, had  $C_{2v}$  symmetry). As a further comparison, interaction

**Table 1.** Interaction Energy,  $\Delta E$ , for  $K^+ \cdots OH_2$  Binding<sup>a</sup>

geometry	basis	method	$\Delta E$	$\Delta E$ (CPC)
HF/6-31G*	6-31G*	HF	−20.29	−18.76
HF/6-31G*	6-311++G(3df,3pd)	MP2	−17.47	−17.18
HF/6-31G*	6-311++G(3df,3pd)	CCSD	−17.31	−17.03
HF/6-31G*	6-311++G(3df,3pd)	BLYP	−16.57	−16.44
BLYP/6-311++G(3df,3pd)	6-311++G(3df,3pd)	BLYP	−16.68	−16.56
HF/6-31G*	pw (70 Ry)	BLYP	−16.50	N/A
HF/6-31G*	pw (140 Ry)	BLYP	−16.62	N/A
HF/6-31G*	pw (280 Ry)	BLYP	−16.62	N/A
HF/6-31G*	6-311++G(3df,3pd)	PW91	−17.69	−17.55
PW91/6-311++G(3df,3pd)	6-311++G(3df,3pd)	PW91	−17.82	−17.68
HF/6-31G*	pw (70 Ry)	PW91	−17.25	N/A
HF/6-31G*	pw (140 Ry)	PW91	−17.37	N/A
HF/6-31G*	pw (280 Ry)	PW91	−17.37	N/A
fixed charge		fixed charge	−18.9	
D <sub>6.5</sub>		Drude model	−17.7	
D <sub>6.8</sub>		Drude model	−17.9	
expt. <sup>a</sup>		Drude model	−18.3 <sup>b</sup>	

<sup>a</sup> Reference 10. <sup>b</sup> Interaction energy estimated from an experimentally measured enthalpy, −17.9 kcal/mol plus −0.4 kcal/mol taken from Drude model computations of the monohydrate enthalpy (see Table 3). <sup>c</sup> In kcal/mol. Interaction energies are compared from quantum chemical basis set computations, classical force fields, and experiment. Unless otherwise noted, the quantum chemical interaction energies are presented for geometries optimized at the HF/6-31G\* level. Data are presented both with and without counterpoise corrections (CPC) to the basis set superposition error (BSSE).

**Table 2.** Optimized Geometries for  $K^+ \cdots OH_2$ <sup>a</sup>

theory level	$r_{OK^+}$	$r_{OH}$	$\theta_{HOH}$
HF/6-31G*	2.6481	0.9511	105.03
BLYP/6-311++G(3df,3pd)	2.6395	0.9736	104.16
PW91/6-311++G(3df,3pd)	2.6116	0.9709	104.06
fixed charge	2.6243	0.9572	104.52
Drude (D <sub>6.8</sub> )	2.6196	0.9572	104.52

<sup>a</sup> Distances are reported in Å; energies are reported in kcal/mol.

energies have also been computed for DFT optimized geometries (see Tables 1 and 2). The resulting geometries are summarized in Table 2. The monohydrate interaction energies for these geometries, at various levels of theory,<sup>61</sup> are presented in Table 1, with and without the Boys–Bernardi counterpoise correction to basis set superposition error.<sup>62</sup> The experimental gas-phase enthalpy for this system has been measured to be −17.9 kcal/mol<sup>10</sup> (see Table 3 and footnote to Table 1).

The interaction energies presented in Table 1 demonstrate the variability and accuracy of the various quantum chemical approaches that have subsequently been applied to larger aqueous  $K^+$  clusters. The interaction energies in Table 1 are all roughly in accord with the experimental estimate of −18.3 kcal/mol (see footnote to Table 1), though there are small differences that deserve to be noted. Nearly all of the quantum chemical interaction energies appear to be slightly less negative than the experimental estimate. The Hartree–Fock calculation, which overestimates the binding by as much as ∼2 kcal/mol, is the lone exception to this rule. Previous analysis showed that the larger binding energy is directly related to the overestimated dipole of the water

**Table 3.** Hydration Enthalpy,  $\Delta H$ , for Gas-Phase  $K^+$   $(H_2O)_n$  Clusters<sup>c</sup>

$n$	fixed charge	Drude $D_{6.8}$	exp. <sup>a</sup>	exp. <sup>b</sup>
1	$-18.5 \pm 0.02$	$-17.5 \pm 0.04$	-17.9	-18.1
2	$-35.6 \pm 0.03$	$-33.0 \pm 0.04$	-34.0	-34.2
3	$-51.2 \pm 0.05$	$-46.2 \pm 0.05$	-47.2	-47.4
4	$-64.3 \pm 0.06$	$-57.7 \pm 0.05$	-59.0	-59.2
5	$-74.6 \pm 0.07$	$-67.0 \pm 0.06$	-69.7	-69.9
6	$-84.4 \pm 0.08$	$-76.0 \pm 0.08$	-79.7	-79.9

<sup>a</sup> Reference 10. <sup>b</sup> Reference 12. <sup>c</sup> In kcal/mol.

molecule, due to neglect of electron correlation.<sup>3</sup> The fixed charge  $K^+$  monohydrate, which was originally parametrized to give a reasonable bulk hydration free energy in TIP3P,<sup>8</sup> also overestimates the monohydrate binding energy. As expected, the counterpoise corrections become smaller for larger basis sets.

In order to assess both the magnitude of the fluctuations in the potential energy within the first hydration shell of  $K^+$  and the level of consistency with which these are represented by various computational models, a series of  $K^+$   $(H_2O)_n$  clusters was examined and compared. First, the enthalpy of hydration,  $\Delta H$ , is reported in Table 3 for a series of  $K^+$   $(H_2O)_n$  clusters with  $1 \leq n \leq 6$  using simulations based on the fixed charge TIP3P and Drude polarizable force fields (model  $D_{6.8}$ ). The enthalpy of the small clusters of one  $K^+$  ion and  $n$  water molecules were calculated as,  $\Delta H = (\langle U_n \rangle - nk_B T)$ , where  $\langle U_n \rangle$  is the average potential energy of the cluster estimated from a 1 ns trajectory at a temperature of 300 K. Examination of Table 3 indicates that the experimentally observed trend is reproduced by both models (more accurately by the polarizable model), although neither model reproduces the experimental gas-phase data exactly.

In addition, the energy of instantaneous snapshots of water molecules surrounding  $K^+$  extracted from a simulation generated using the polarizable force field with model  $D_{6.8}$  was calculated and compared for the various models. Configurations with  $4 \leq n \leq 7$  were extracted. For each configuration, all the O- $K^+$  distances were within a 3.5 Å radius from the  $K^+$ , serving here as the standard definition of the first hydration shell of the ion (see above). The ranking of cluster interaction energies for the instantaneous configurations, shown in Figure 1, follows that for the  $K^+$  monohydrates, with a few variations. Interestingly, both the polarizable ( $D_{6.8}$ ) and the fixed charge model closely follow the trends of the quantum chemical interaction energies. While both models yield similar bulk hydration free energies, the polarizable  $D_{6.8}$  model is in closer agreement with the MP2 and PW91 (with an atom-centered basis set) interaction energies for this set of configurations. Despite the difference in magnitude, the energies of the instantaneous snapshots are highly correlated. A normalized correlation coefficient can be defined as

$$C_{ij} = \frac{\langle \Delta E_i \Delta E_j \rangle}{\sqrt{\langle \Delta E_i^2 \rangle \langle \Delta E_j^2 \rangle}} \quad (3)$$

where  $\Delta E_i = E_i - \langle E_i \rangle$ . The  $C_{ij}$  vary between 0.94 (e.g., Drude with HF/6-31G\*) to 0.99 (e.g., Drude with MP2, or

Drude with PW91) for all the models. The high degree of correlation suggests that, while the magnitude of the energies are different, the structure of the potential energy surface is similar in all the models.

**B. Hydration Free Energy.** The hydration free energy provides an important reference to assess the validity of various models. The Lennard-Jones parameters of  $K^+$  were explored to ascertain the sensitivity of the polarizable potential energy function. Lennard-Jones parameters could not be found to generate polarizable models of  $K^+$  which had both very small O- $K^+$  monohydrate distances and lower interaction energies. As is evident in Figure 2, it was nevertheless possible to find polarizable models for  $K^+$  that had hydration numbers of  $\sim 6.5$ . Looking at both Figures 2 and 3, it is observed that polarizable models for  $K^+$  that have a hydration number of  $\sim 6.5$  also have hydration free energies of about -77 kcal/mol. The hydration free energy of a set of  $Na^+$  models was also calculated to assess the consistency, or lack thereof, with the putative  $K^+$  models. The absolute  $Na^+$  hydration free energies are shown in Figure 4. This consistency is important because, while there are inherent uncertainties concerning the absolute scale of single-ion hydration free energy, the relative hydration free energy between monovalent cations is known from experiment very accurately.<sup>12</sup> The relative hydration free energy between  $K^+$  and  $Na^+$  from experiments is 17.2 kcal/mol.<sup>12</sup>

From an exploration of the  $\{U_{\min}, d_{\min}\}$  space for aqueous hydration of  $K^+$ , two models were selected for further study: one which accurately captures the monohydrate geometry and interaction energy ( $U_{\min}, d_{\min} = (-17.9$  kcal/mol, 2.62 Å), and another which sacrifices some of this accuracy in order to yield a hydration number that is in closer accord with that predicted by a recent analysis of neutron scattering experiments, ( $U_{\min}, d_{\min} = (-17.7$  kcal/mol, 2.59 Å). The first model has a hydration number of 6.8, while the second model has a coordination number of 6.5 (integrating the radial distribution functions up to a distance of 3.5 Å). These two polarizable models are referred to as  $D_{6.8}$  and  $D_{6.5}$ , respectively. They are indicated in Figures 2 and 3. As an example of how these Drude models must work in conjunction with other Drude polarizable ions, consider a Drude model of  $Na^+$  that can be matched with the  $D_{6.8}$  model of  $K^+$ :  $D_{6.8}$  has a hydration free energy of  $\Delta G_{\text{hydr}} = -80.15$  kcal/mol. Any Drude model for  $Na^+$  that has a hydration free energy of  $\Delta G_{\text{hydr}} = -97.35$  kcal/mol (representable as a contour in Figure 4) might be suitable. The best choice, however, would also accurately reproduce the monohydrate properties.<sup>5</sup> In this case, a Drude  $Na^+$  model with ( $U_{\min}, d_{\min} = (-24.0$  kcal/mol, 2.288 Å) is an optimal choice. For the  $D_{6.5}$  model of  $K^+$ , with a hydration free energy of  $\Delta G_{\text{hydr}} = -76.60$  kcal/mol, a Drude model for  $Na^+$  would be found along the  $\Delta G_{\text{hydr}} = -93.80$  kcal/mol contour of Figure 4. While such a model can be found for  $Na^+$ , it lies close to the boundary of physically realizable models in the ( $U_{\min}, d_{\min}$ ) variables (see Figure 4): it is not possible in general to find a reasonable Drude model of  $Na^+$  that is consistent with an arbitrarily chosen  $K^+$  model.

The hydration free energy for the PW91 and BLYP models are estimated to be -74.3 and -66.1 kcal/mol using a



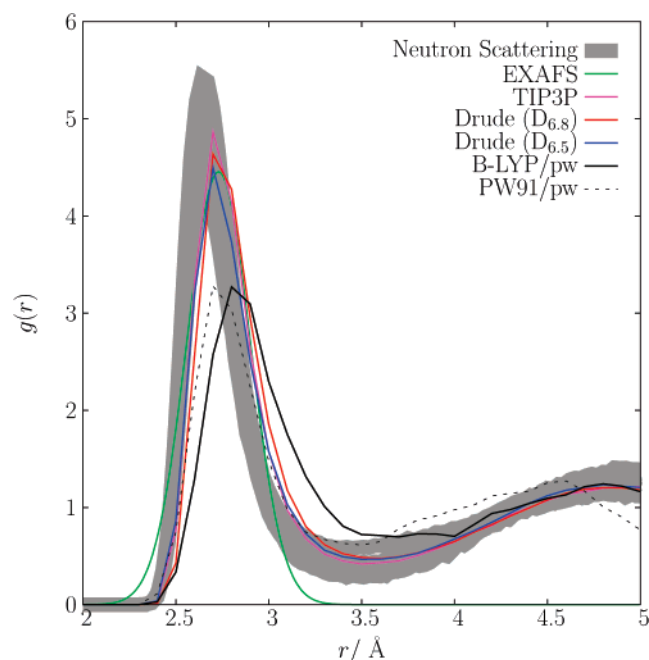


**Figure 5.** Radial distribution function extracted from the analysis of neutron scattering experimental data<sup>13</sup> and different simulations based on the fixed charge model, two polarizable models, and the BLYP/pw and PW91/pw models. The position of the main peak is as follows: neutron data, 2.65; TIP3P, 2.71;  $D_{6.8}$ , 2.71;  $D_{6.5}$ , 2.71; BLYP, 2.83; PW91, 2.73 (in Å). The Gaussian radial distribution function extracted from EXAFS (mean at 2.73 Å and width 0.1712 Å), normalized to a coordination number of 6, is also shown.<sup>63</sup>

computational scheme based on the quasi-chemical theory.<sup>20</sup> In this computational scheme, the  $K^+$  ion and the 4 nearest water molecules (within  $\sim 3.0$  Å, see Figure 6) are modeled explicitly with the exchange-correlation density functional, while the influence of the remaining liquid is incorporated via a far-field treatment. Dispersion interactions and packing effects have been neglected in these particular estimates. These effects are expected to contribute with opposite signs and yield an overall slightly less favorable hydration free energy. It is also worth noting that the quasi-chemical estimates for the BLYP and PW91 density functionals are based on ab initio computations including all electrons, differing slightly with the models of the BOMD and CPMD simulations, which represent the core electrons using a pseudopotential. Superficially, these estimates appear to differ from the molecular dynamics based free energy perturbation (FEP/MD) calculations based on the potential functions by as much as 14 kcal/mol, but this is deceptively incorrect. The FEP/MD calculations with SSBP include the phase potential arising from the vacuum-liquid interface (e.g., they are *real* hydration free energies),<sup>5</sup> whereas the calculations carried out according to the quasi-chemical theory report the *intrinsic* hydration free energy. In calculations based on potential functions, the phase potential is on the order of  $-500$  mV in the liquid, thus contributing favorably to the solvation of a cation by about 12 kcal/mol.<sup>5</sup> Adding this contribution from potential functions to the estimated *intrinsic* hydration free energy based on the quasi-chemical theory yields a *real* hydration free energy on the order of

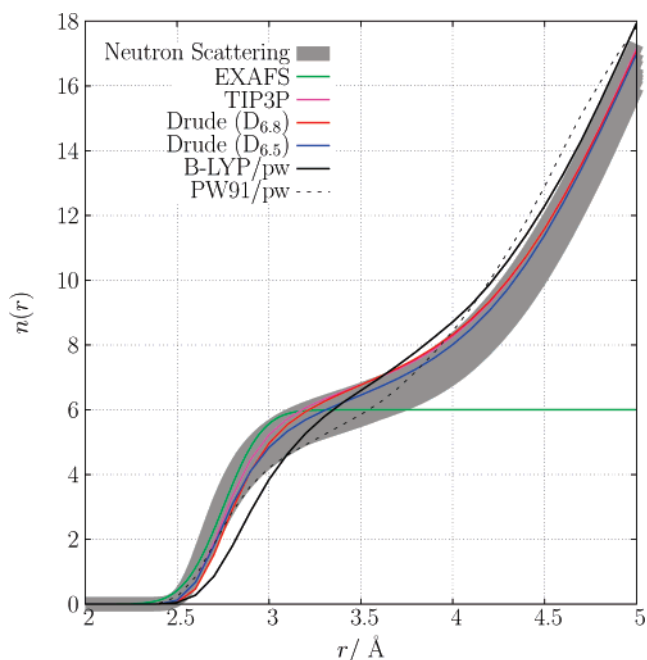


**Figure 6.** Hydration number,  $n(r)$ , of  $K^+$  contact from several different models: the fixed charge model, two polarizable models, and the BLYP/pw and PW91/pw models. The coordination number is as follows: neutron data, 5.5–6.4; TIP3P, 6.77;  $D_{6.8}$ , 6.8;  $D_{6.5}$ , 6.5; BLYP, 6.6; PW91, 5.86 (all integrated up to a distance of 3.5 Å). The hydration number  $n(r)$  estimated from EXAFS is also shown.<sup>63</sup>

about  $-86$  kcal/mol for the PW91 approximate exchange-correlation functional or a little less if packing and dispersion effects are incorporated. While further work would be required to ascertain the validity of this comparison, the present analysis suggests that the hydration free energy from the  $D_{6.8}$  polarizable model is consistent with the value obtained from the quasi-chemical treatment.

**C. Hydration Structure in the Bulk Liquid.** The radial distribution functions,  $g(r)$ , for the O– $K^+$  contact, for each of the computational models studied here, are presented in Figure 5, along with recently reported radial distributions extracted from neutron scattering experimental data.<sup>13</sup> In order to gauge the spread in the experimental data, they are presented as a set of overlapping distributions, each one deduced from neutron scattering measurements on  $K^+$  solutions made with different salts (KF, KCl, KBr, and KI) and of different concentrations (data for a total of 12 different solutions are shown). The radial distribution of the fixed charge model, based upon TIP3P water, agrees closely with that of the  $D_{6.8}$  model. The  $D_{6.5}$  model, adjusted to yield a slightly lower coordination number, remains within the range of the experimentally refined distributions. All the radial distribution functions are peaked around 2.7–2.8 Å, though the distributions from the two ab initio simulations (BLYP and PW91) are clearly more diffuse and less sharply peaked than those from classical simulations (TIP3P and Drude polarizable models). On average, the position of the peak in  $g(r)$  is shifted outward by about 0.10 Å relative to the energy minimum ion–water oxygen distance in the monohydrate (Table 2), except for BLYP/pw where it is shifted by almost 0.2 Å. It is worth noting that the distribution functions

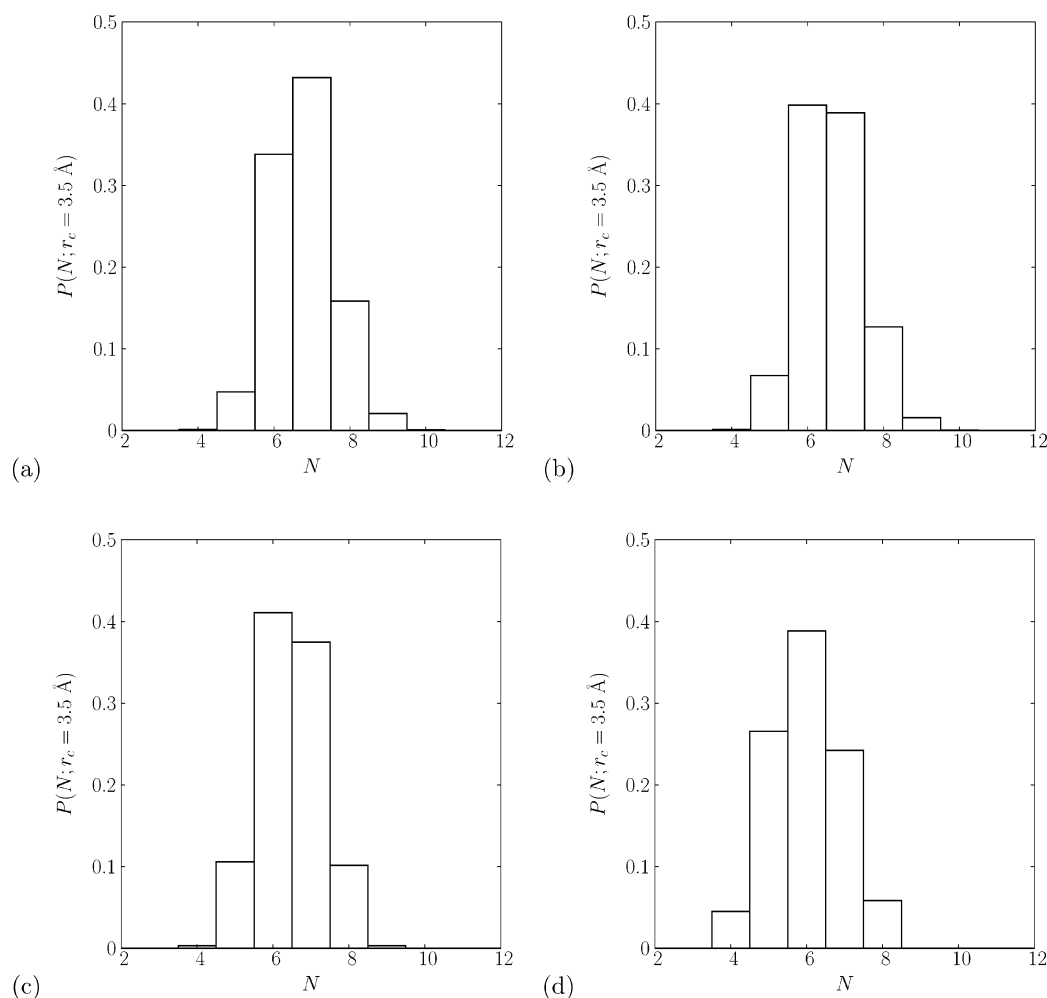


**Figure 7.** The probability distributions,  $P(N; r_c = 3.5 \text{ \AA})$ , for the hydration number of aqueous  $\text{K}^+$  in the (a) fixed charge, (b) Drude polarizable ( $\text{D}_{6.8}$ ), and (c) BLYP/pw and (d) PW91/pw descriptions of the system.

extracted from neutron scattering were also obtained from classical simulations, which were constrained to fit the experimental data.<sup>13</sup> An estimate of the first peak (represented as a Gaussian) based on an analysis of the anomalous diffraction of  $\text{K}^+$  by X-ray absorption fine structure (EXAFS) spectra is also shown.<sup>63</sup>

The hydration numbers for  $\text{K}^+$  in each of the computational models as well as those deduced from experiments are presented in Figure 6. A  $3.5 \text{ \AA}$  radial cutoff, which is near the minimum between the first and second peaks in  $g(r)$ , is used throughout to define a unique standard for comparing the calculated coordination number of aqueous  $\text{K}^+$  (see earlier discussion). Recently reported hydration numbers deduced from neutron diffraction experiments<sup>13</sup> range from  $5.5 \leq n(r_c = 3.5 \text{ \AA}) \leq 6.4$ . The estimated hydration number from EXAFS is  $6 \pm 1$ .<sup>63</sup> Earlier experiments had estimated this number anywhere from 4 to 8 water molecules in the first shell.<sup>14</sup> Density functional models estimate the hydration number to be slightly below (PW91) or above 6 (BLYP). The coordination numbers are 6.77 and 6.8, for TIP3P and  $\text{D}_{6.8}$ , respectively. Although the computational models studied here all differ in their details, the calculated number of water molecules in the first hydration shell consistently lies within the range of what can currently be estimated from experiment.

In Figure 7, the probability distribution,  $P(N; r_c = 3.5 \text{ \AA})$ , of finding  $N$  water molecules that have their oxygen atoms within  $3.5 \text{ \AA}$  from the ion is presented for the different models. In BLYP/pw and PW91/pw ab initio simulations, the number of water molecules found with the highest probability within the first hydration shell is 6. For the polarizable model  $\text{D}_{6.8}$ , the probability distribution has a maximum at 6, while it is 7 for the fixed charge model. The maximum of  $P(N; r_c = 3.5 \text{ \AA})$  is 6 for the BLYP/pw simulation, partly due to the use of the  $r_c = 3.5 \text{ \AA}$  cutoff. As can be seen from Figure 5, a  $r_c = 3.75 \text{ \AA}$  cutoff would be closer to the minimum, and, indeed this larger cutoff was previously determined by Ramaniah et al.<sup>54</sup> in their simulation using the same BLYP approximate exchange-correlation functional and semicore  $\text{K}^+$  pseudopotential that has been employed here. If a cutoff of  $r_c = 3.75 \text{ \AA}$  is used, the maximum in  $P(N)$  becomes 7 for the BLYP/pw simulation.

The fluctuations about the mean hydration number offer a measure of the dynamics within the coordination shell of solvent surrounding  $\text{K}^+$ . Remarkably, all of the distributions in Figure 7 are well described by Gaussian distributions with similar variances. The standard deviation for the fixed charge model is  $\sigma_N = 0.86$ , for the  $\text{D}_{6.8}$  model it is  $\sigma_N = 0.86$ , while for the ab initio models it is  $\sigma_N = 0.84$  and  $\sigma_N = 0.96$  for BLYP/pw and PW91/pw, respectively. Thus, while the mean



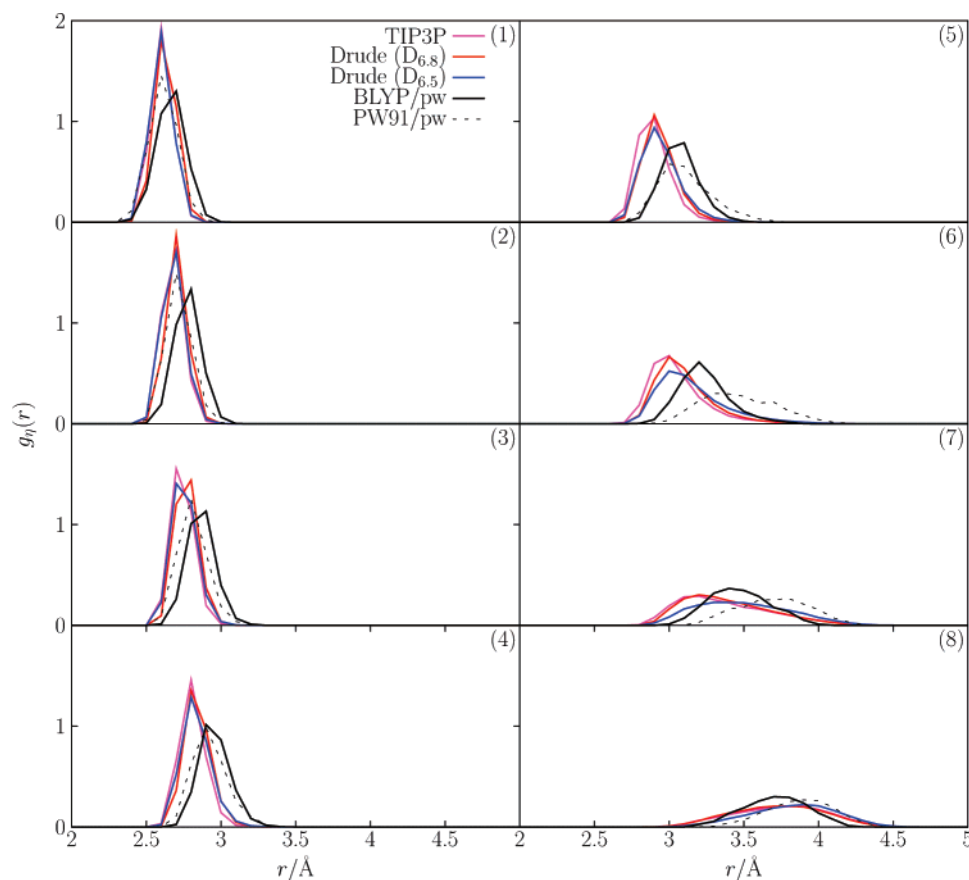


**Figure 8.** Partial radial distribution functions of the O– $K^+$  contact for the fixed charge, Drude ( $D_{6.8}$ ) polarizable, and BLYP/pw and PW91/pw descriptions of the system. The panels contain partial radial distribution functions for the (1) nearest contact, (2) next nearest, (3) third nearest, (4) fourth, (5) fifth, (6) sixth, (7) seventh, and (8) eighth nearest contact.

coordination number varies slightly among the different models, coordination states within  $\pm 1$  water molecules about the mean occur approximately 70% of the time in all the models. The significant fluctuations in coordination suggests that the hydration structure around  $K^+$  is quite dynamic. This is expected, as the density at the minimum between the first and second hydration shell ( $r = 3.5$  Å) is about 50–60% of the bulk solvent density.

A useful way to characterize the hydration structure of an ion is to examine “partial” radial distribution functions. For example, the radial distribution function of whichever oxygen atom is closer to the  $K^+$  ion than is any of the other oxygen atoms in the system, or whichever oxygen is the second closest, and so on. For each such partial radial distribution function, the radial integral converges to 1 at some finite distance, by construction. In Figure 8, the partial radial distribution functions for each of the first 8 nearest oxygen atoms are presented. The differences between the various descriptions of aqueous  $K^+$  that were apparent in the  $g(r)$  are also seen in the partial radial distribution functions. On average the two ab initio simulations display a looser hydration structure than the classical models, with the third- to sixth-nearest contacts shifted to larger separations, though they also display some differences with one another. This is especially noticeable for the O– $K^+$  distances of the first- to fourth-nearest contacts of BLYP/pw, which are further on average than for those of PW91/pw. The fixed charge partial radial distributions are closely matched with those of the  $D_{6.8}$

and  $D_{6.5}$  polarizable models. The partial radial distribution functions from the BLYP/pw and PW91/pw simulations are similar to one another for the 5 nearest water molecules around  $K^+$ . For the sixth-, seventh-, and eighth-nearest O– $K^+$  contacts, the PW91/pw coordination structure is looser compared with that of BLYP/pw—that is, the oxygen atoms of these three partial radial distributions are further from the  $K^+$  ion in the PW91/pw representation of this system than they are in the BLYP/pw representation.

In addition, Figure 9 displays the cumulative partial hydration numbers for each of the models studied here. From Figure 9, it can easily be seen which of the nearby water molecules is contributing significant density to the radial distribution function features within  $r_c = 3.5$  Å. For example, with the fixed charge model, there are essentially 6 oxygen atoms entirely within the 3.5 Å cutoff; the remainder of the  $n(r_c) = 6.77$  coordination number is contributed by both the seventh- and eighth-nearest water molecules. In the PW91/pw simulation, 5 oxygens lie within the 3.5 Å cutoff, while the sixth- and seventh-nearest water molecules also contribute to the density within the first hydration shell.

**D. Self-Diffusion of  $K^+$ .** The diffusion constant of  $K^+$  has been computed for the  $D_{6.5}$  and  $D_{6.8}$  polarizable Drude models from the mean-square displacement. Because there is only a single ion in the system, relatively long simulations are required to obtain well converged estimates. Accordingly, 5 independent simulations of 1 ns length were averaged together for each polarizable model. The diffusion constant

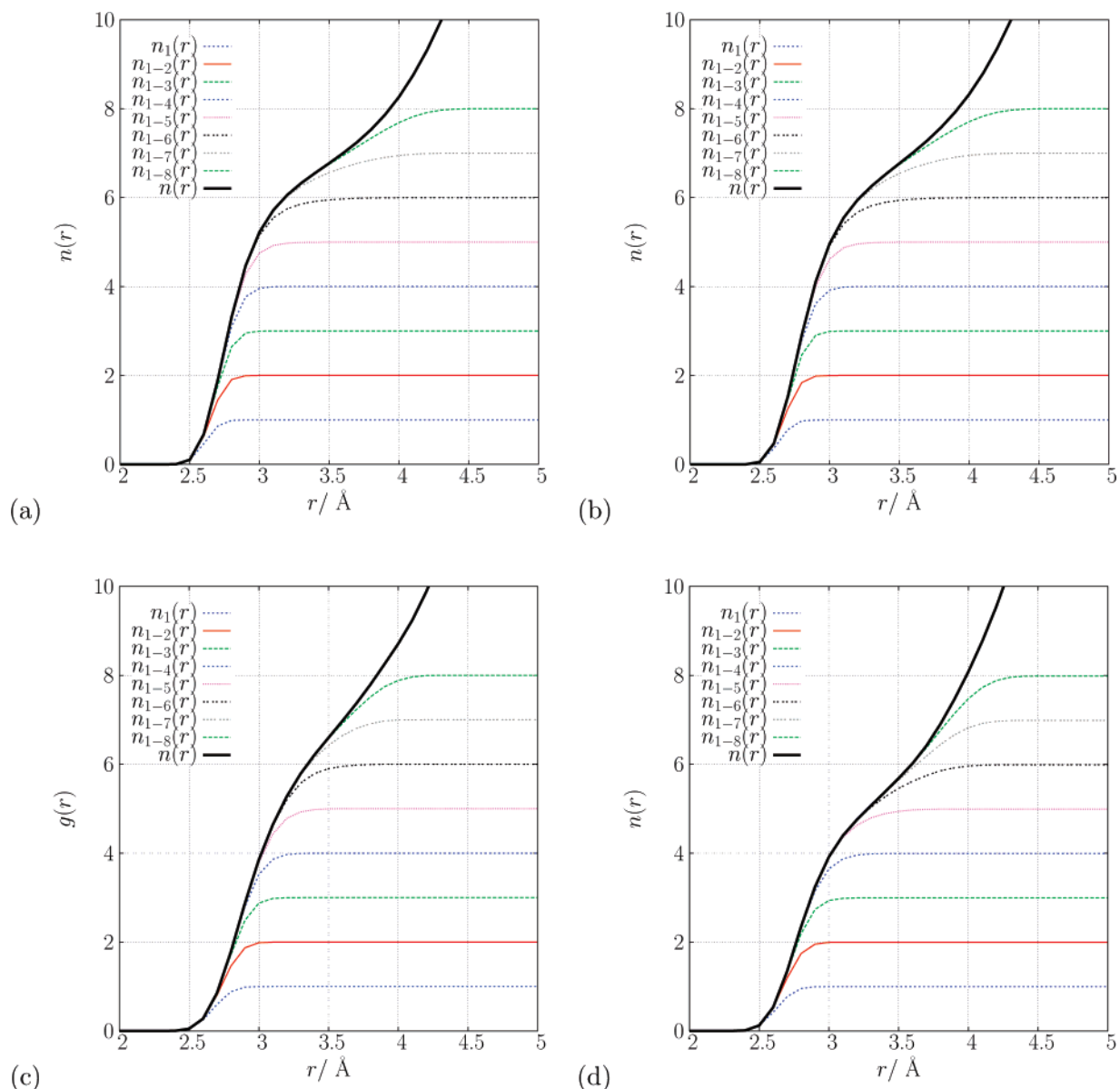


**Figure 9.** Cumulative partial hydration numbers,  $n_{1-a}(r)$ , of aqueous  $K^+$  in the (a) fixed charge, (b) Drude polarizable ( $D_{6.8}$ ), and (c) BLYP/pw and (d) PW91/pw descriptions of the system.

of the  $D_{6.5}$  model was  $1.71 \pm 0.2 \times 10^{-5} \text{ cm}^2/\text{s}$ , and for the  $D_{6.8}$  model it was  $1.83 \pm 0.2 \times 10^{-5} \text{ cm}^2/\text{s}$ . Both of these values are in excellent agreement with the experimental value of  $1.96 \times 10^{-5} \text{ cm}^2/\text{s}$ .<sup>64</sup> One may note that, in this particular case, the model with the lower hydration number actually diffuses slightly more slowly (though the difference is very small). However, a systematic analysis of a family of models shows that the diffusion coefficient does tend to decrease when the hydration number increases (by about  $-0.092 \times 10^{-5} \text{ cm}^2/\text{s}$ ), in accord with the expected hydrodynamic trend).

**E. Electronic Polarization near and far from  $K^+$ .** The induction effects of the  $K^+$  ion on its first hydration shell were compared between the polarizable model and the ab initio models by computing the respective distributions of molecular dipole magnitudes. For models of neutral molecules based on point charges, calculating the molecular dipole amounts to a straightforward sum over molecular charges. The situation is more ambiguous for ab initio

simulations of condensed-phase systems, where the electronic charge density is continuously distributed. One approach that has been used in the past<sup>65–68</sup> is to transform from the Kohn–Sham orbitals to the basis of maximally localized Wannier functions.<sup>69–71</sup> In the localized basis, the Wannier function centers (WFCs) allow for an assignment of molecular dipoles. In the present study, analysis of the WFCs allows for comparison between the water dipole distributions in the bulk and in the nearest solvation shell as well as between computational models for  $K^+$  hydration.

The effects of polarization within the first hydration shell of  $K^+$  were studied by computing the distribution of molecular dipole magnitudes for water molecules within the first hydration shell and for those outside. The molecular dipoles in the CPMD simulation were assigned using the WFCs, and the distributions are shown in Figure 10. In total, WFCs were computed for 94 different configurations of the equilibrated BLYP/pw system. These configurations were taken from the final 47 ps of the production run, and each

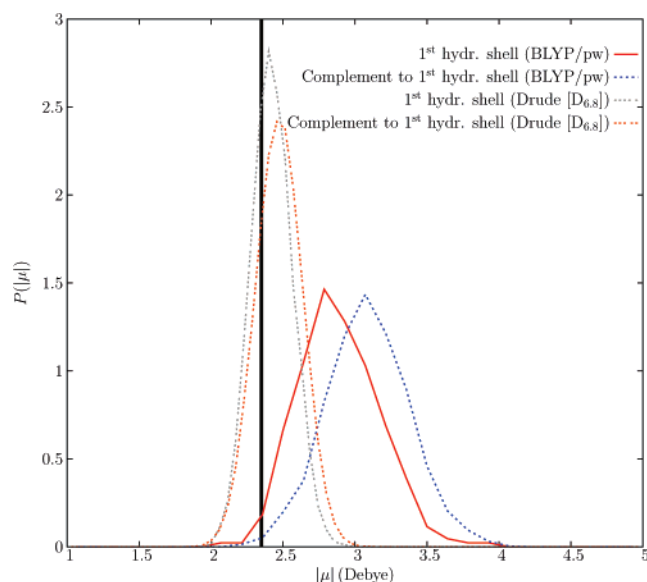


**Figure 10.** Probability distributions of molecular dipole magnitudes,  $P(|\mu|)$ , for water molecules in the aqueous  $K^+$  system. Distributions are shown for water molecules in the first hydration shell, defined by a 3.5 Å O– $K^+$  distance, and for water molecules outside of the first hydration shell, for the Drude polarizable, and BLYP/pw descriptions, respectively. For reference, the vertical line at  $|\mu| = 2.35$  Debye indicates the magnitude of the TIP3P molecular dipole.

was 500 fs apart from the next. The average dipole magnitude for water molecules outside of the first hydration shell is consistent with previously reported pure liquid water values for both the SWM4-NDP<sup>25</sup> and BLYP/pw.<sup>66</sup> Of particular interest, there is a small downward shift in the average dipole magnitude for water molecules within the first hydration shell for both the BLYP/pw and Drude polarizable models. The shift is 0.2 Debye and 0.05 Debye for the BLYP/pw and the  $D_{6.8}$  polarizable models, respectively. Relative to the value of the average molecular dipole magnitude in the bulk,  $\delta\langle|\mu|\rangle/\langle|\mu|\rangle$ , the shifts are 6.5% in the BLYP/pw simulation and 2% in the polarizable force field simulation. A qualitatively similar shift has been observed by comparing, for a polarizable force field model, the distribution of molecular dipole magnitudes in  $K^+$  ( $H_2O$ )<sub>n</sub> clusters with that in pure bulk water.<sup>72</sup>

The observation that the molecular dipole of water within the first hydration shell of  $K^+$  has a slightly smaller average value than that in bulk water is rather counterintuitive. A water molecule in the first hydration shell would be expected to be polarized by the electric field from the ion. This is certainly observed for a  $K^+$  monohydrate, but the situation is more complex in the bulk phase. The surprising electrostatic properties revealed by Figure 10 result from a balance of competing factors. There is a net benefit to align the water molecules and induce dipoles within the first hydration shell. There is also an unfavorable energy cost arising from the interaction between those dipoles pointing toward a central point. Furthermore, the molecular dipole of water increases from the vapor to the liquid phases due to the hydrogen-bonding network structure of liquid water.<sup>73–75</sup> As this network is disrupted in the neighborhood of  $K^+$ , the average

magnitude of the molecular dipole decreases.<sup>67</sup> Finally, it is worth noting that, because the shift in the  $\langle|\mu|\rangle$  is small, fixed charged models like TIP3P closely approximate the hydration structure of the polarizable models near  $K^+$ . This may partly explain the surprising ability of nonpolarizable models to represent bulk hydration of ions.

**F. On Differences and Similarities.** The present study shows that our current knowledge of  $K^+$  hydration is satisfactory, with different models being in broad agreement with the available experimental data. The interaction energy of the monohydrate is about  $-18$  kcal/mol, near the experimental gas-phase estimate. The hydration structure in the bulk is consistent with a coordination number on the order of 6–7 and with a first peak around 2.7 Å, as indicated by the analysis of neutron scattering from solutions. The total solvation free energy is about  $-80$  kcal/mol, consistent with a variety of thermodynamic estimates from experiments<sup>12,15,16,40,41</sup> or computations.<sup>4–9</sup> In comparison, the AMOEBA model of Grossfield, Ren, and Ponder<sup>4</sup> yields a *real* hydration free energy for  $K^+$  that is roughly 4–5 kcal/mol larger than the present estimate and a coordination number of 7.0. Such differences appear to be within acceptable bounds.

Nevertheless, at a finer level, there remain some discrepancies that should be better understood to further refine our models of ion hydration. For example, there are notable differences between the position and the shape of the main peak extracted from the neutron scattering data and the results from the two ab initio simulations (see Figure 5). The average radial distribution function extracted from neutron scattering for 12 solutions is sharply peaked at 2.65 Å, whereas the peak from the two ab initio simulations are more diffuse. In the case of the simulation based on BLYP, the peak is also slightly shifted toward larger distances. What is puzzling is the fact that the two classical models (including the non-polarizable force field) are in closer agreement with the results from neutron scattering experiments than the two ab initio simulations. Normally, the average coordination structure obtained from ab initio simulations is quite reliable. However, it is important to keep in mind that the radial distribution functions are extracted from the neutron scattering data using a refinement procedure, which relies on a set of simulations biased to fit the experiments.<sup>13</sup> Those simulations are not not exempt from assumptions. For example, the  $K^+$ -oxygen minimum distance is set to 2.6 Å (Alan Soper, personal communication), based on an earlier estimate from Herdman and Neilson.<sup>76</sup> Furthermore, the ion–water repulsion is modeled after a Lennard-Jones potential, which is generally steeper than the core repulsion calculated from ab initio. In spite of these caveats, the  $g(r)$  extracted from the neutron scattering data shown in Figure 5 is in reasonable accord with a variety of experimental X-ray and neutron scattering data indicating that the peak in the  $K^+$ -oxygen distribution function should be somewhere between 2.60 and 2.80 Å (though some older estimates were as high as 2.92 Å).<sup>77</sup> Furthermore, the coordination number extracted from the neutron scattering data via the refinement procedure, ranging from 5.5 to 6.4, appears to be nearly reproduced by all the models (see Figure 6). In excellent accord with the

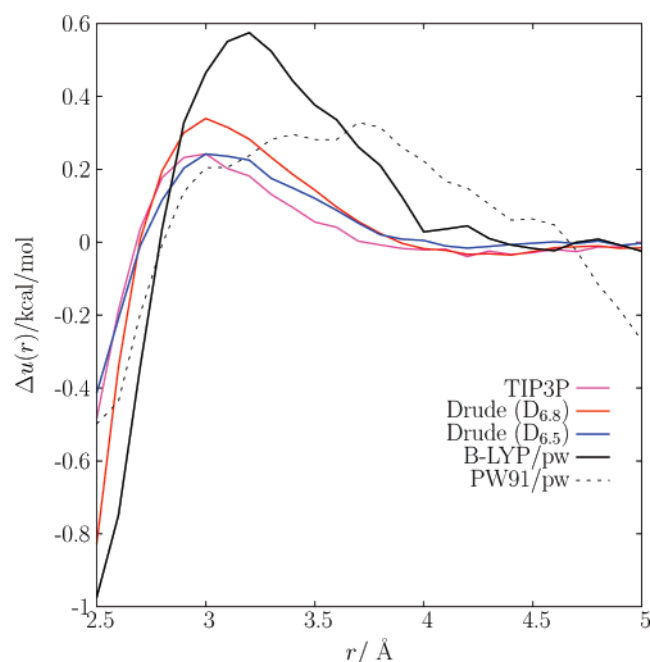


**Figure 11.** Perturbative analysis of the  $\text{K}^+$ -water oxygen interaction using the average radial distribution function extracted from the neutron scattering data as a reference.

current results, a recent estimate based on an analysis of the anomalous diffraction of  $\text{K}^+$  by X-ray absorption fine structure (EXAFS) spectra estimates the average distance between the  $\text{K}^+$  and the water oxygen in the first shell at  $2.730 \pm 0.05$  Å and the coordination number at  $6 \pm 1$ .<sup>63</sup>

While an assessment of the sensitivity of the results extracted from neutron scattering data to all input assumptions would be required to ascertain the accuracy of the different computational models, an important question remains whether the observed differences in the radial distribution functions signal some fundamental underlying problems in our understanding of  $\text{K}^+$  hydration. At the simplest level, differences in the radial distribution of  $\text{K}^+$ -water oxygen observed in Figure 5 could be caused simply by differences in the direct ion–water interaction. Such small differences, on the order of  $\sim 0.5$  kcal/mol, can already be noted in Table 1. In fact, nearly all the ab initio calculations yield a  $\text{K}^+$ -water binding energy that is slightly weaker than the experimental estimate (the exception being the HF/6-31G\* calculation). By a low order perturbative treatment, one can express the small differences observed between the various radial distribution functions from the various models in terms of a putative difference in the direct ion–water interaction. Taking the average radial distribution function extracted from the neutron scattering data as a reference  $g_{\text{ref}}(r)$ , we define the potential  $\Delta u_i(r)$

$$\Delta u_i(r) = -k_{\text{B}}T \ln \left[ \frac{g_{\text{ref}}(r)}{g_i(r)} \right] \quad (4)$$

To lowest order,  $\Delta u_i(r)$  is the potential that needs to be added to the ion–water interaction of a model  $i$  in order to recover  $g_{\text{ref}}(r)$ . Of course, such analysis is valid only if the perturbation is small. At higher order, the ability of a liquid to coordinate an ion is also related to the amount of cohesion

that exists in the pure liquid, e.g., hydration of an ion would be reduced in a water model that attributes more internal cohesion to the liquid, and it should be increased in a model that attributes less cohesion to the liquid. Nonetheless, an analysis based on eq 4 is informative. The results for  $\Delta u_i(r)$  are plotted in Figure 11. According to this perturbative analysis, it appears that all the models (except the ab initio simulations from BLYP), would require a fairly small perturbation in the ion–water interaction to yield  $g_{\text{ref}}(r)$ . At near-contact ( $r \approx 2.6$ – $2.7$  Å), the perturbation amounts to a fraction of kcal/mol, which is consistent with the magnitude of the variations observed in the binding energy of the monohydrates given in Table 1. From this perspective, it is possible that the differences observed between the various models might reflect the relatively small differences in the direct ion–water interaction.

## IV. Conclusion

A hierarchy of computational models have been used to study the properties of aqueous  $\text{K}^+$ , including two ab initio models, a fixed charge model, and a polarizable model based on classical Drude oscillators. The O– $\text{K}^+$  radial distribution functions of the models have been compared with those derived from neutron scattering experiments.<sup>13</sup> Among the different computational representations of the system, the polarizable model and fixed charge model appear to agree more closely with the shape of the radial distribution functions deduced from experiments, while those from the two ab initio simulations seems to be not as sharply peaked. All the computational models yield hydration number between 5.86 (PW91/pw) and 6.8 ( $\text{D}_{6.8}$ ), in good accord with the experimental estimates (see Figure 6), and yield a reasonable monohydrate binding energy as well as hydration free energy.

A somewhat counterintuitive observation made on the basis of the  $\text{D}_{6.8}$  and CPMD simulations concerns the induced dipolar of water molecules nearest to the  $\text{K}^+$ . The electronic polarization effects of the  $\text{K}^+$  ion on the water molecules in the first hydration shell have been examined using a BLYP/pw ab initio simulation and a polarizable force field simulation of aqueous  $\text{K}^+$ . In both cases, a slight shift to lower average dipole magnitudes for molecules in the first hydration shell, compared to that in the bulk liquid, has been observed. This observation contradicts the intuitive notion that water molecules in direct contact with a cation must be overpolarized compared to the bulk value. In fact, it appears that in the case of  $\text{K}^+$  they are, if anything, slightly less polarized than the water molecules in the bulk. This is, perhaps, one reason for the relative success of simple fixed charged models.<sup>6–9</sup> It may be that  $\text{K}^+$  has a size that renders it similar to water in its “polarizing strength”, suggesting that only smaller ions require a treatment of induced polarization. In view of this result, one might be tempted to suggest that a polarizable force field is not really needed for  $\text{K}^+$ . In the context of a homogeneous bulk liquid phase, this is partly true. However, one must be careful in overextending this conclusion to inhomogeneous environments such as interfaces or the interior of narrow pores. In those systems,



the limitations of nonpolarizable force fields in the case of  $K^+$  have been clearly documented.<sup>78</sup>

Although a fairly consistent perspective of  $K^+$  hydration emerges from the current study, resolving a number of issues could further our ability in modeling ion hydration accurately. In particular, a sensitivity analysis of the hydration structure properties extracted from scattering experimental data would be very useful. Contrasting the results from different computational models also helps delineate the limits of present knowledge about  $K^+$  hydration. Simulations based on quantum mechanical ab initio methods can account for a wide range of complex electronic effects. But the complete information about the thermodynamic properties in the bulk phase of those ab initio models is not easily accessible to ascertain the implications of the results. The properties in the bulk phase can be fully explored for computationally simpler models based on a potential function, such as the polarizable force field based on Drude oscillators. Such models use parametrized mathematical functional forms to represent complex microscopic interactions. While those parameters can be freely adjusted to reproduce various properties for any cation, the structure of the potential function places internal constraints on the range of possible models that can be constructed. This idea is illustrated in Figures 2–4. In the present study, the coordination numbers of  $K^+$  and  $Na^+$  are strongly correlated with the monohydrate binding energies and thus with the bulk hydration free energies. This correlation was illustrated here by considering two different polarizable models for  $K^+$ . One model, referred to as  $D_{6.8}$ , was fitted to agree with the  $K^+$  monohydrate properties. The other model, referred to as  $D_{6.5}$ , was adjusted to interact less strongly with water, in order to yield a lower hydration number in closer accord with the ab initio simulations. However, the hydration free energy of the  $D_{6.5}$  model of  $K^+$  is decreased, and it becomes challenging to parametrize a model of  $Na^+$  with a relative hydration free energy that is consistent with the experiment.<sup>12,40,41</sup> Thus, in the context of the polarizable potential function based on classical Drude oscillators, the relative hydration free energy of  $K^+$  and  $Na^+$  (or any other ion) limits the range of accessible coordination numbers. Such internal constraints deduced from simulations based on a given functional form of force field are model-specific. Nonetheless, qualitatively similar observations are made from the AMOEBA model of  $K^+$ , where a slightly larger coordination number is correlated with a slightly larger hydration free energy.<sup>4</sup> This correlation suggests that such internal constraints qualitatively reflect inherent trends (e.g., one cannot arbitrarily shift the first peak in  $g(r)$  to larger distances and expect to decrease the hydration number while reproducing the monohydrate properties and achieving a reasonable hydration free energy), though particular results could change quantitatively if a different functional form was used. Thus, development of a microscopic perspective on  $K^+$  hydration, integrating the information provided by experiments and computational models, remains partly subjective at this point.

**Acknowledgment.** We are very grateful to Alan K. Soper for sharing his recently published<sup>13</sup> data and for insightful comments. T.W.W. thanks Mark E. Tuckerman

for sharing the potassium pseudopotential and G.J. Martyna for helpful discussions. T.W.W. is supported by a strategic LDRD grant from Argonne National Laboratory. This work was funded by the National Institutes of Health through the NIH Roadmap for Medical Research, award number PHS 2 PN2 EY016570B, and the grant GM072558 (B.R.). Sandia is a multiprogram laboratory operated by Sandia Corporation, a Lockheed Martin Company, for the U.S. Dept. of Energy. This work was also supported by the LDRD program under Contract DE-AC04-94A185000.

## Appendix: Analysis of Statistical Error and Finite Size Effects

The statistical error in the radial distribution functions calculated from the BLYP/pw simulation was determined by dividing the 50 ps trajectory into 25 2 ps parts and calculating the error in the mean of each histogram window,  $r$ , to generate  $\Delta(r) = \sigma(r)/\sqrt{25}$ , the  $r$ -dependent error in  $g(r)$ . This estimate compares well with a more accurate one obtained by performing 50 simulations of length 40 ps (the same length as the BOMD simulation) using the Drude force field and computing  $\Delta(r) = \sum_k \sigma^{(k)}(r)/50$ . In Figure 12, the radial distribution function computed from each of the 50 independent 40 ps simulations is plotted along with the average  $g(r)$ . The spread in the distributions in Figure 12 gives an excellent estimate of the statistical uncertainty from a short simulation (also shown are the error bars resulting from the above analysis of the Drude model trajectories).

In order to assess the significance of finite size effects in the relatively small system containing 64 water molecules, the radial distribution function for the O– $K^+$  contact is compared, in Figure 13, with that generated from a much

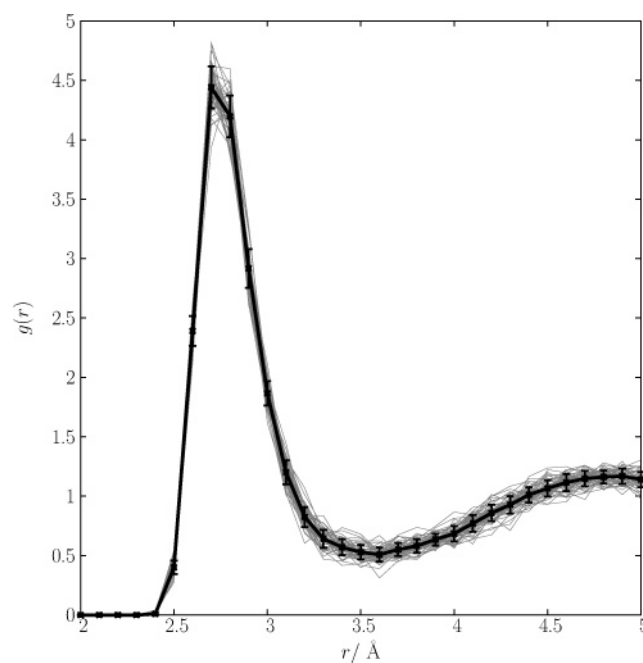


**Figure 12.** Statistical spread in  $g(r)$  of the O– $K^+$  contact taken from 40 ps of molecular dynamics. The Drude polarizable model was used to simulate the system. The black line is the average  $g(r)$ .

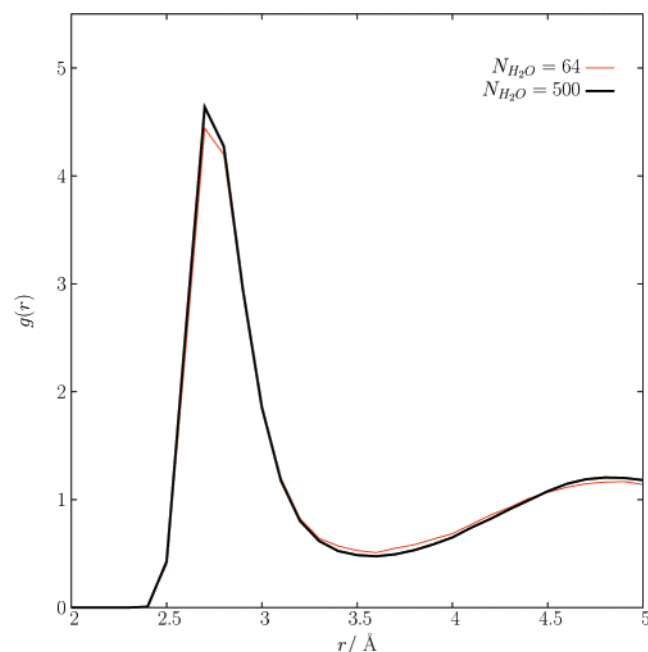


**Figure 13.** Radial distribution function of the O–K<sup>+</sup> contact taken from two different system sizes: a smaller system with 64 water molecules and a larger system containing 500 water molecules. Both system sizes were modeled using the Drude D<sub>6.8</sub> polarizable force field.

larger system containing 500 water molecules. In both cases, it is a polarizable model system that is being simulated. It is evident that finite size effects are not significant for this property of aqueous K<sup>+</sup>.

### References

- (1) Lybrand, T. P.; Kollman, P. A. *J. Chem. Phys.* **1985**, *83*, 2923–2933.
- (2) Dang, L. X.; Rice, J. E.; Caldwell, J.; Kollman, P. A. *J. Am. Chem. Soc.* **1991**, *113*, 2481–2486.
- (3) Roux, B.; Karplus, M. *J. Comput. Chem.* **1995**, *16*, 690–704.
- (4) Grossfield, A.; Ren, P.; Ponder, J. W. *J. Am. Chem. Soc.* **2003**, *125*, 15671–15682.
- (5) Lamoureux, G.; Roux, B. *J. Phys. Chem. B* **2006**, *110*, 3308–3322.
- (6) Jorgensen, W. L.; Tirado-Rives, J. *J. Am. Chem. Soc.* **1988**, *110*, 1657–1666.
- (7) Åqvist, J. *J. Phys. Chem.* **1990**, *94*, 8021–8024.
- (8) Beglov, D.; Roux, B. *J. Chem. Phys.* **1994**, *100*, 9050–9063.
- (9) Jensen, K. P.; Jorgensen, W. L. *J. Chem. Theory Comput.* **2006**, *2*(6), 1499–1509.
- (10) Džidić, I.; Kebarle, P. *J. Phys. Chem.* **1970**, *74*, 1466–1474.
- (11) Klassen, J. S.; Anderson, S. G.; Blades, A. T.; Kebarle, P. *J. Phys. Chem.* **1996**, *100*, 14218–14227.
- (12) Tissandier, M. D.; Cowen, K. A.; Feng, W. Y.; Gundlach, E.; Cohen, M. H.; Earhart, A. D.; Coe, J. V.; Tuttle, T. R., Jr. *J. Phys. Chem. A* **1998**, *102*, 7787–7794.
- (13) Soper, A. K.; Weckström, K. *Biophys. Chem.* **2006**, *124*, 180–191.
- (14) Varma, S.; Rempe, S. B. *Biophys. Chem.* **2006**, *124*, 192–199.
- (15) Gomer, R.; Tryson, G. *J. Chem. Phys.* **1977**, *66*, 4413–4424.
- (16) Klots, C. E. *J. Phys. Chem.* **1981**, *85*, 3585–3588.
- (17) Zhan, C.-G.; Dixon, D. A. *J. Phys. Chem. A* **2001**, *105*, 11534–11540.
- (18) Asthagiri, D.; Pratt, L. R.; Ashbaugh, H. S. *J. Chem. Phys.* **2003**, *119*, 2702–2708.
- (19) Beck, T. L.; Paulaitis, M. E.; Pratt, L. R. *The Potential Distribution Theorem And Models Of Molecular Solutions*; Cambridge University Press: Cambridge, MA, 2006.
- (20) Pratt, L. R.; Rempe, S. B. In *Simulation and Theory of Electrostatic Interactions in Solution: Computational Chemistry, Biophysics, and Aqueous Solutions*; number 492 in AIP Conference Proceedings, Pratt, L. R., Hummer, G., Eds.; American Institute of Physics: New York, 1999; pp 172–201.
- (21) Pérez-Jordá, J. M.; San-Fabián, E.; Pérez-Jiménez, A. J. *J. Chem. Phys.* **1999**, *110*, 1916–1920.
- (22) Zimmerli, U.; Parrinello, M.; Koumoutsakos, P. *J. Phys. Chem.* **2004**, *120*, 2693–2699.
- (23) Tao, J.; Perdew, J. P. *J. Chem. Phys.* **2005**, *122*, 114102.
- (24) Jorgensen, W. L.; Chandrasekhar, J.; Madura, J. D.; Impey, R. W.; Klein, M. L. *J. Chem. Phys.* **1983**, *79*, 926.
- (25) Lamoureux, G.; Harder, E.; Vorobyov, I. V.; Roux, B.; MacKerell, A. D., Jr. *Chem. Phys. Lett.* **2006**, *418*, 245–249.
- (26) Drude, P. *Lehrbuch der Optik*; S. Hirzel: Leipzig, Germany, 1900.
- (27) Sangster, M. J. L.; Dixon, M. *Adv. Phys.* **1976**, *25*, 247.
- (28) Stillinger, F. H.; David, C. W. *J. Chem. Phys.* **1978**, *69*, 1473.
- (29) Pratt, L. R. *Mol. Phys.* **1980**, *40*, 347.
- (30) Sprik, M.; Klein, M. L. *J. Chem. Phys.* **1989**, *89*, 7556.
- (31) Lamoureux, G.; Roux, B. *J. Chem. Phys.* **2003**, *119*, 3025.
- (32) Wang, Y.; Perdew, J. P. *Phys. Rev. B* **1991**, *44*(24), 13298–13307.
- (33) Perdew, J. P.; Chevary, J. A.; Vosko, S. H.; Jackson, K. A.; Pederson, M. R.; Singh, D. J.; Fiolhais, C. *Phys. Rev. B* **1992**, *46*(11), 6671–6687.
- (34) Becke, A. D. *Phys. Rev. A* **1988**, *38*, 3098–3100.
- (35) Lee, C.; Yang, W.; Parr, R. G. *Phys. Rev. B* **1988**, *37*, 785–789.
- (36) Essmann, U.; Perera, L.; Berkowitz, M. L.; Darden, T.; Lee, H.; Pedersen, L. G. *J. Chem. Phys.* **1995**, *103*, 8577.
- (37) Martyna, G. J.; Klein, M. L.; Tuckerman, M. *J. Chem. Phys.* **1992**, *97*, 2635–2643.
- (38) Ryckaert, J. P.; Ciccotti, G.; Berendsen, H. J. C. *J. Comput. Phys.* **1977**, *23*, 327–341.
- (39) Allen, M. P.; Tildesley, D. J. *Computer Simulation of Liquids*; Oxford University Press: Oxford, 1987.
- (40) Noyes, R. M. *J. Am. Chem. Soc.* **1962**, *84*, 513–522.
- (41) Marcus, Y. *Biophys. Chem.* **1994**, *51*, 111–127.
- (42) Deng, Y.; Roux, B. *J. Phys. Chem. B* **2004**, *108*, 16567–16576.

- (43) Kumar, S.; Bouzida, D.; Swendsen, R. H.; Kollman, P. A.; Rosenberg, J. M. *J. Comput. Chem.* **1992**, *13*, 1011–1021.
- (44) Kresse, G.; Hafner, J. *Phys. Rev. B* **1993**, *47*(1), 558–561.
- (45) Kresse, G.; Furthmüller, J. *Phys. Rev. B* **1996**, *54*(16), 11169–11186.
- (46) Car, R.; Parrinello, M. *Phys. Rev. Lett.* **1985**, *55*, 2471.
- (47) Samuelson, S.; Martyna, G. J. *J. Chem. Phys.* **1998**, *109*, 11061–11073.
- (48) Tuckerman, M. E.; Yarne, D.; Samuelson, S. O.; Hughes, A. L.; Martyna, G. J. *Comput. Phys. Commun.* **2000**, *128*, 333–376.
- (49) Varma, S.; Rempe, S. B. *Biophys. J.* **2007**, *93*.
- (50) Blöchl, P. E. *Phys. Rev. B* **1994**, *50*(24), 17953–17979.
- (51) Kresse, G.; Joubert, D. *Phys. Rev. B* **1999**, *59*(3), 1758–1775.
- (52) Berendsen, H. J. C.; Grigera, J. R.; Straatsma, T. P. *J. Phys. Chem.* **1987**, *91*, 6269–6271.
- (53) Troullier, N.; Martins, J. L. *Phys. Rev. B* **1991**, *43*, 1993–2006.
- (54) Ramaniah, L. M.; Bernasconi, M.; Parrinello, M. *J. Chem. Phys.* **1999**, *111*, 1587–1591.
- (55) Tassone, F.; Mauri, F.; Car, R. *Phys. Rev. B* **1994**, *50*(15), 10561–10573.
- (56) Tuckerman, M. E.; Parrinello, M. *J. Chem. Phys.* **1994**, *101*, 1302–1315.
- (57) Tuckerman, M. E.; Parrinello, M. *J. Chem. Phys.* **1994**, *101*, 1316–1329.
- (58) Hutter, J.; Tuckerman, M. E.; Parrinello, M. *J. Chem. Phys.* **1995**, *102*, 859–871.
- (59) Martyna, G. J.; Tuckerman, M. E.; Tobias, D. J.; Klein, M. L. *Mol. Phys.* **1996**, *87*, 1117–1157.
- (60) Brooks, B. R.; Bruccoleri, R. E.; Olafson, B. D.; States, D. J.; Swaminathan, S.; Karplus, M. *J. Comput. Chem.* **1983**, *4*, 187–217.
- (61) Frisch, M. J.; Trucks, G. W.; Schlegel, H. B.; Scuseria, G. E.; Robb, M. A.; Cheeseman, J. R.; Montgomery, J. A., Jr.; Vreven, T.; Kudin, K. N.; Burant, J. C.; Millam, J. M.; Iyengar, S. S.; Tomasi, J.; Barone, V.; Mennucci, B.; Cossi, M.; Scalmani, G.; Rega, N.; Petersson, G. A.; Nakatsuji, H.; Hada, M.; Ehara, M.; Toyota, K.; Fukuda, R.; Hasegawa, J.; Ishida, M.; Nakajima, T.; Honda, Y.; Kitao, O.; Nakai, H.; Klene, M.; Li, X.; Knox, J. E.; Hratchian, H. P.; Cross, J. B.; Bakken, V.; Adamo, C.; Jaramillo, J.; Gomperts, R.; Stratmann, R. E.; Yazyev, O.; Austin, A. J.; Cammi, R.; Pomelli, C.; Ochterski, J. W.; Ayala, P. Y.; Morokuma, K.; Voth, G. A.; Salvador, P.; Dannenberg, J. J.; Zakrzewski, V. G.; Dapprich, S.; Daniels, A. D.; Strain, M. C.; Farkas, O.; Malick, D. K.; Rabuck, A. D.; Raghavachari, K.; Foresman, J. B.; Ortiz, J. V.; Cui, Q.; Baboul, A. G.; Clifford, S.; Cioslowski, J.; Stefanov, B. B.; Liu, G.; Liashenko, A.; Piskorz, P.; Komaromi, I.; Martin, R. L.; Fox, D. J.; Keith, T.; Al-Laham, M. A.; Peng, C. Y.; Nanayakkara, A.; Challacombe, M.; Gill, P. M. W.; Johnson, B.; Chen, W.; Wong, M. W.; Gonzalez, C.; Pople, J. A. *Gaussian 03, Revision 02*; Gaussian, Inc.: Pittsburgh, PA.
- (62) Boys, S. F.; Bernardi, F. *Mol. Phys.* **1970**, *19*, 553–566.
- (63) Glezakou, V.-A.; Chen, Y.; Fulton, J. L.; Schenter, G. K.; Dang, L. X. *Theor. Chem. Acc.* **2006**, *115*, 86–99.
- (64) Lide, D. R., Ed. *CRC Handbook of Chemistry and Physics*, 87th ed.; Taylor and Francis: Boca Raton, FL, 2007.
- (65) Silvestrelli, P. L.; Parrinello, M. *Phys. Rev. Lett.* **1999**, *82*, 3308–3311.
- (66) Silvestrelli, P. L.; Parrinello, M. *J. Chem. Phys.* **1999**, *111*, 3572–3580.
- (67) Boero, M.; Terakura, K.; Ikeshoji, T.; Liew, C. C.; Parrinello, M. *Phys. Rev. Lett.* **2000**, *85*(15), 3245–3248.
- (68) Whitfield, T. W.; Crain, J.; Martyna, G. J. *J. Chem. Phys.* **2006**, *124*, 094503.
- (69) Wannier, G. H. *Phys. Rev.* **1937**, *52*, 191–197.
- (70) Foster, J. M.; Boys, S. F. *Rev. Mod. Phys.* **1960**, *32*, 300–302.
- (71) Resta, R.; Sorella, S. *Phys. Rev. Lett.* **1999**, *82*, 370–373.
- (72) Carrillo-Tripp, M.; Saint-Martin, H.; Ortega-Blake, I. *J. Chem. Phys.* **2003**, *118*, 7062–7073.
- (73) Bernal, J. D.; Fowler, R. H. *J. Chem. Phys.* **1933**, *1*, 515.
- (74) Stillinger, F. H. *Science* **1980**, *25*, 451–547.
- (75) Chen, B.; Ivanov, I.; Klein, M. L.; Parrinello, M. *Phys. Rev. Lett.* **2003**, *91*, 215503.
- (76) Herdman, G. J.; Neilson, G. W. *J. Mol. Liq.* **1990**, *46*, 165–179.
- (77) Marcus, Y. *Chem. Rev.* **1988**, *88*, 1475–1498.
- (78) Roux, B.; Berneche, S. *Biophys. J.* **2002**, *82*, 1681–1684.

CT700172B